Published in final edited form as:
Inorg Chem. 2009 August 3; 48(15): 7117–7126. doi:10.1021/ic900307f.

Macrocyclic Diamide Ligand Systems: Potential Chelators for ^{64}Cu- and ^{68}Ga-Based Positron Emission Tomography Imaging Agents

Peter J. Barnard[†,*,§], **Jason P. Holland**[†], **Simon R. Bayly**[†], **Thaddeus J. Wadas**[‡], **Carolyn J. Anderson**[‡], and **Jonathan R. Dilworth**[†,*]

[†]Department of Chemistry, Inorganic Chemistry Laboratory, University of Oxford, South Parks Road, Oxford OX1 3QR, U.K.

[‡]Mallinckrodt Institute of Radiology, Washington University School of Medicine, 510 South Kings highway Boulevard, Campus Box 8225, St. Louis, Missouri 63110

Abstract

The N_4-macrocyclic ligand 2,10-dioxo-1,4,8,11-tetraazabicyclo[11.4.0]1,12-heptadeca-1(12), 14,16-triene H_2**L** has been synthesized by the [1 + 1] condensation reaction between *N*,*N*′-bis(chloroacetyl)-1,2-phenylenediamine and 1,3-propylenediamine. The coordination chemistry of this ligand has been investigated with the metal ions Cu (II), Ni(II), Zn(II), and Ga(III) (complexes **1**, **2**, **3** and **4**, respectively). H_2**L** and its metal complexes have been fully characterized by the use of NMR, UV/vis, electron paramagnetic resonance, and elemental analysis where appropriate. The four metal complexes **1**–**4** have been structurally characterized by X-ray crystallography which confirmed that in all cases the amide nitrogen atoms are deprotonated and coordinated to the metal center. Complexes **3** and **4** are five-coordinate with a water molecule and chloride ion occupying the apical site, respectively. Cyclic voltammetric measurements on complex **1** show that this complex is oxidized reversibly with a half-wave potential, $E_{1/2}$ = 0.47 V, and reduced irreversibly at E_P = −1.84 V. Density functional theory calculations reproduce the geometries of the four complexes. The one-electron reduction and oxidation potentials for **1** were calculated by using two solvent models, DMF and H_2O. The calculations indicated that the one electron oxidation of **1** may involve removal of an electron from the ligand as opposed to the metal center, producing a diradical. The diamide macrocyle is of interest for the development of new positron emission tomography (PET) and single photon emission computed tomography (SPECT) imaging agents, and a radiolabeled complex has been synthesized with the positron emitting isotope ^{64}Cu. In vivo biodistribution studies for the ^{64}Cu labeled complex, ^{64}Cu-**1**, in male Lewis rats, showed that the activity is cleared rapidly from the blood within 1–2 h post-administration.

[*]To whom correspondence should be addressed. p.barnard@latrobe.edu.au (P.J.B.), jon.dilworth@chem.ox.ac.uk (J.R.D.).
[§]Present address: Department of Chemistry, La Trobe University, Victoria, 3086, Australia

Supporting Information Available: Further details are given in Figures S1–S3 and Tables S1–S4. This material is available free of charge via the Internet at http://pubs.acs.org.

Introduction

There is considerable interest in the development of new bifunctional ligands for use in the preparation of targeted molecular imaging agents based on metallic radionuclides. In our laboratory we have been investigating new chelating agents for a range of nuclides including ^{64}Cu ($t_{1/2}$ = 12.7 h) and ^{68}Ga ($t_{1/2}$ = 68 min) for positron emission tomography (PET) and ^{99m}Tc ($t_{1/2}$ = 6.0 h) for single photon emission computed tomography (SPECT).

A major focus of our research has been the development of copper(II) complexes of *bis*(thiosemicarbazonato) ligands (Cu(II)-BTSCs) as imaging agents for tumor hypoxia.[1–4] The mechanism by which Cu(II)-BTSCs accumulate in hypoxic tissue is believed to involve a bioreductive process,[2,5–10] where the neutral Cu(II) species enters cells by passive diffusion and is reduced to Cu(I) by biological reducing agents. The fate of this Cu(I) complex then depends on the structure of the bis-thiosemicarbazone ligand and the tissue oxygen concentration. Normal oxygen levels leads to rapid reoxidation of the Cu(I) complex, while in regions of hypoxia the Cu(I) compound persists and may undergo protonation and/or ligand dissociation leading to transmetalation of the Cu(I) ion from the BTSC ligand to copper chaperone proteins.[11]

Generally, the development of molecular imaging agents targeted to sites of interest in vivo using bioactive peptides or monoclonal antibodies (mAbs) require that the radio-metal complex has high thermodynamic and kinetic stability.[12] High in vivo stability is advantageous as it allows the imaging agent to achieve the desired target tissue biodistribution and optimum clearance characteristics from tissues where no target receptor sites are found. However, it has been demonstrated that a high formation constant alone cannot be relied upon as an indicator of high in vivo stability. For example, we have evaluated the 14-membered macrocycle (cyclam) derivative TETA (Figure 1) as a carrier for ^{64}Cu using in vivo studies.[13] Despite the high thermodynamic formation constant (log K = 21.9)[12,14] for the Cu(II) complex of TETA, there is significant loss of ^{64}Cu from both ^{64}Cu(TETA) and its bioconjugates in vivo.[15,16] A similar reductive mechanism to that of Cu(II)-BTSCs, where Cu(II) is initially reduced followed by loss of Cu(I) from the chelate, has been proposed to account for the instability of Cu(II)-TETA and its bioconjugates in vivo.[17]

In an effort to generate imaging agents based on Cu(II) that display increased stability in vivo, we have been developing new ligands that stabilize copper in the divalent oxidation state, thus avoiding the loss of copper as a result of reductive processes. Deprotonated amide nitrogen (amidato) donors are well-known for their propensity to stabilize metal ions in higher oxidation states. Early studies by Margerum and co-workers demonstrated that Cu(II) and Ni(II) complexes of small peptides where the amide nitrogen atoms were deprotonated and coordinated to the metal ion could be readily oxidized.[18–21] In addition a series of linear N_4-tetradentate and macrocyclic ligands containing deprotonated amide donors have been shown to stabilize a range of metal ions in higher oxidation states.[22–25]

Here we report the synthesis of a N_4-macrocyclic ligand, 2,10-dioxo-1,4,8,11-tetraazabicyclo[11.4.0]1,12-heptadeca-1 (12),14,16-triene, H_2**L** and its Cu(II), Ni(II), Zn(II)

and Ga(III) complexes. The ligand has been radiolabeled with ^{64}Cu, and the in vivo biodistribution of the ^{64}Cu labeled complex has been investigated in male Lewis rats.

Results and Discussion

Synthesis

The N_4-macrocyclic ligand H_2**L**[27] was synthesized by the [1 + 1] condensation reaction between *N*,*N*′-bis(chloroacetyl)-1,2-phenylenediamine and 1,3-propylenediamine (Scheme 1). The use of the acyclic bis (α-chloroamide) intermediate was based on a procedure initially described by Bradshaw et al.[26] A series of aliphatic dioxotetraamines of radiopharmaceutical interest[28] have been synthesized from bis(α-chloroamide)s and a series of tosylated diamines.[29] Our interest in the phenyl linker over a purely aliphatic system was prompted first by the ease with which this group can be derivatized, allowing for the potential conjugation of biologically active molecules. Second, the aromatic group allows for facile synthesis of the macrocycle without the use of template conditions.

The Cu(II), Ni(II), Zn(II), and Ga(III) complexes of H_2**L** were prepared by the treatment of a equimolar mixture of the ligand and the chloride salts of the metal ions in refluxing methanol with 3 equiv of sodium methoxide (Scheme 2). In all cases these conditions caused deprotonation and coordination of the ligand amide nitrogen atoms. While there are numerous examples of Cu(II) and Ni(II) complexes with deprotonated amide nitrogen donors, Zn(II) and Ga(III) complexes displaying this type coordination mode are rare.[30,31]

Spectroscopic Studies

The ^{1}H and ^{13}C NMR data for H_2**L**, **2**, **3**, and **4** are given in the experimental section and were assigned by using two-dimensional COSY, HMQC, and HMBC experiments. The proligand H_2**L** exhibits a pair of sharp multiplets with an AA′XX′ pattern for the aromatic protons. In contrast, broadening of the peaks is observed for the CH_2 groups of the propylene linker indicating a degree of restricted movement in this unit. The amide NH protons were not observed for H_2**L** in $(CD_3)_2SO$, possibly as a result of broadening. Complexes **2**, **3**, and **4** display similar ^{1}H NMR spectra consistent with rigid species, with no exchange of proton environments on the NMR time scale. The geminal and vicinal couplings exhibited for the propylene chain are consistent with a six-membered ring comprising the two amine donors and the metal center adopting a chair configuration. The different magnetic environments above and below the plane described by the four nitrogen donors is also evidenced from the different chemical shifts exhibited by the protons of the methylene units. Temperature dependence studies (298–373 K) for the nickel complex **2** did not result in a simplification of the ^{1}H spectrum, indicating a significant barrier to inversion of the propylene chain.

X-ray Structural Studies

The single crystal X-ray structures of complexes **1–4** were determined, and the crystallographic data for complexes **2**, **3**, and **4** are given in Table 1. The molecular structures of these species are shown in Figure 2, and selected bond lengths and angles are given in Table 2. The X-ray diffraction studies confirm that in each case the ligand is

coordinated the metal via the two deprotonated amide nitrogen atoms and the two amine nitrogen atoms, with these donor atoms sitting in an essentially planar arrangement. The structure of complex **1** determined in this work was found to be the same as that reported previously (monoclinic $P2_1/n$),[27] and a representation of the structure is included in Figure 2 for comparison (the data does not appear in the Table 1). The coordination geometry of the Cu(II) center is slightly distorted from planarity with the Cu(II) ion displaced above the least-squares plane defined by the four nitrogen atoms by 0.225 Å on the side *cis* with respect to the amine NH groups. This distortion appears to be associated with a cation-π interaction with the phenyl ring of a neighboring molecule, as indicated by the relatively short Cu(1)···C(11) (symmetry operator $1 - x, 1 - y, 1 - z$) distance of 2.972(5) Å. In the case of complex **2**, the Ni(II) ion sits in an essentially square-planar coordination environment with a slight displacement from the least-squares plane defined by the four nitrogen atoms of 0.096 Å on the side *trans* with respect to the amine NH groups. In each case the amine groups are hydrogen bonded to a carbonyl oxygen atoms of adjacent molecules with N(3)···O(1) (symmetry operator $x, 1 - y, -1/2 + z$) = 2.790(6) Å and N(2)···O(2) (symmetry operator $1.5-x, 1/2 + y, 1/2-z$) = 3.058(6) Å. Disorder was identified from residual electron density in the difference map (Table 1) and was also evident from comparison of the anisotropic displacement parameters for N(2) and N(3) to those of N(1) and N(4). It is likely that the disorder results from the two possible chair-type configurations of the six-membered ring, that is, ring-flip disorder. Efforts were made to model this disorder. However, the occupancy of the minor component refined to less than 3%, and the refinement was found to be unstable. For complex **3** the Zn(II) ion lies in a pseudo square-pyramidal geometry with the four nitrogen donor atoms of the ligand lying in a square-planar arrangement and a water molecule occupying the fifth apical site. The Zn(II) ion is displaced above the least-squares plane defined by the four nitrogen atoms by 0.654 Å toward the coordinated water molecule. A hydrogen bonding interaction exists between the coordinated water of one molecule and the amide carbonyl oxygen atoms of two adjacent molecules with O(4)···O(1) (symmetry operator $1/2 - x, 1 - y, 1/2 + z$) = 2.629(3) Å and O(4)···O(2) (symmetry operator $1 - x, 1/2 + y, 1.5 - z$) = 2.645(3) Å. In addition a water molecule of crystallization is also hydrogen bonded to these amide carbonyl oxygen atoms with O(3)···O(1) (symmetry operator $1/2 - x, 1 - y, 1/2 + z$) = 2.869(3) Å and O(3)···O(2) (symmetry operator $1 + x, y, z$) = 2.859(3) Å.

The Ga(III) complex **4** has no crystallographic symmetry, but has an approximate local mirror plane. The four coordinated nitrogen atoms are approximately coplanar, with the Ga(III) ion displaced from the least-squares plane by 0.560 Å toward a coordinated chloride ion. The two amine groups form hydrogen bonds to carbonyl oxygen atoms of neighboring molecules N(2)···O(2) (symmetry operator $-1/2 + x, 1.5 - y, -1/2 + z$) = 2.823(2) Å, N(3)···O(1) (symmetry operator $1/2 - x, 1/2 + y, 1/2 - z$) = 2.827(2) Å. The solvent (methanol) hydroxyl group also forms a hydrogen bond to a carbonyl oxygen atom O(3)···O(1) = 2.823(2) Å. The hydrogen bonds form infinite sheets running parallel to the crystallographic $(1\,0\,\bar{1})$ planes.

Electrochemistry

The electrochemical properties of complex **1** were studied by using cyclic voltammetry, and the cyclic voltammogram of a solution of complex **1** (5.0×10^{-3} M) in anhydrous DMF recorded at 200 mV s^{-1} with $^{n}Bu_4NBF_4$ (0.10 M) supporting electrolyte using a platinum disk working electrode and a platinum wire auxiliary electrode is shown in Figure 3. The quasi-reversible oxidation wave ($E_{1/2}$(SCE) = + 0.473 V, ΔE_p = 91 mV, and $|i_a|/|i_c|$ = 1.02) was assigned to the one-electron oxidation of the ligand to give a radical cation $[\mathbf{1}]^{+\bullet}$. The scan rate dependence of the oxidation wave is shown in Figure S1 (Supporting Information), and the inset plot of peak currents i_p/μA versus the square root of scan rate $\upsilon^{1/2}/(\mathrm{mV/s^{-1}})^{1/2}$ shows a linear relationship, confirming reversibility of the couple. Assignment of the couple to the formation of the triplet state as opposed to oxidation at the metal center to give the singlet state was made on the basis of spectroelectrochemical experiments and DFT calculations (see below). An irreversible reduction peak was also observed, which is assigned to a one electron Cu(II/I) process with E_p = −1.84 V vs SCE (Saturated Calomel Electrode).

Spectroelectrochemistry

UV/visible spectroelectrochemistry (SEC) was used to investigate the nature of the oxidized species by performing in situ electrochemical oxidation ($E_{appl.}$ = 1.13 V (SCE)) and monitoring the changes in the electronic absorption spectra of a solution of **1** (1.0×10^{-3} M) in DMF using an optically transparent thin-layer electrochemical (OTTLE) cell (path-length, l = 0.46 mm). Spectra were recorded between 850–320 nm and are shown in Figure 4. In the spectrum of complex **1**, the peak in the visible region occurs at 467 nm (ε = 33 M^{-1} cm^{-1}). Upon electrochemical oxidation the absorption intensity shows >20 fold increase, with the final ε value being (706 M^{-1} cm^{-1}). Complete conversion of complex **1** to the oxidized form was judged to have occurred when both the current and the spectra were invariant with time and the current was close to zero. The in situ electrogenerated oxidized copper complex was stable in solution throughout the duration of the experiment (Figure 4).

Electron Paramagnetic Resonance Spectroscopy

The simulated and experimental electron paramagnetic resonance (EPR) spectrum of complex **1**, recorded in dimethylformamide (DMF) at room temperature is shown in Figure 5. Simulation of the experimental spectrum using EasySpin[33] gave ^{63}Cu hyperfine splittings (A_{Cu}) of 100 MHz (contributions from ^{65}Cu were not modeled). Couplings from two pairs of ^{14}N nuclei (two amide and two amine donors) were included in the simulation, giving nitrogen superhyperfine lines with A_N(amide) = 16 MHz and A_N(amine) = 10 MHz and g_{iso} = 2.081. A low g_{iso} value of this magnitude is indicative of a high degree of covalency in the coordination complex.

Density Functional Calculations

Density functional theory (DFT) was used to calculate the optimized gas phase geometries of complexes **1–4**. The calculated geometries reproduce the structures determined by single crystal X-ray diffraction with all bond lengths and bond angles (Table 2) being within the standard errors expected for geometry optimizations using the B3LYP exchange-correlation

functionals and the 6–31 + + G(d,p) basis set.[34] The DFT calculated and X-ray diffraction (XRD) bond length between the Zn(II) ion and the coordinated water molecule are significantly different (0.23 Å). It is likely that this difference arises from a combination of inherent errors in the DFT calculations and as a result of the error associated with comparison of experimental solid-state structures with calculated gas-phase systems. The weakly bound water molecule is involved in strong hydrogen bonding interactions which may influence the Zn–O bond length, and this interaction was not modeled by the calculations. The DFT optimized Cartesian coordinates for complexes **1–4** are given in Tables S1–S4 (Supporting Information).

The one-electron reduction and oxidation potentials, *E*(SCE)/V, of **1** were calculated according to previously described procedures.[3] Two solvation models were used to assess the variation in the predicted redox potentials with differing dielectric constants and solvent sphere radius (ε and R_{solv}, respectively). The data are summarized in Table 3. DFT calculations indicate that ligand-based oxidation of **1** giving a cationic species in the triplet state is energetically more favorable than formation of the singlet state by 40.5 kJ mol^{-1}.

The calculated and experimental one-electron reduction of complex **1**, to give $[\mathbf{1}]^-$, occur at highly negative potentials which are inaccessible under biologically relevant conditions. Therefore, the complex is predicted to be both kinetically and thermodynamically stable with respect to reduction and demetalation, a desired characteristic for a potential ^{64}Cu-based radiopharmaceutical.

A variation in the calculated one-electron reduction potential between the water and DMF solvation models is observed, and in both cases the absolute calculated values are underestimated. In DMF a more negative reduction potential is predicted as a result of a less negative change in overall solvation $\Delta\Delta_{solv}G^0$ of −28.2 kJ mol^{-1} in DMF compared to −33.9 kJ mol^{-1} in water. The underestimation of the calculated reduction potential in DMF when compared to the experimental value is likely to occur as a result of the increase in the dielectric constant of the continuum solvation model (PCM), which stabilizes the energy of the anionic species and hence leads to the prediction of a less negative value for the one-electron reduction potential. The DFT results indicate that little change in structure is observed on reduction of complex **1**, and the complex retains a square-planar geometry. The rmsd between the DFT calculated **1** and the reduced $[\mathbf{1}]^-$ structures is only 0.209 Å, whereas the rmsd between the X-ray crystal structure and the $[\mathbf{1}]^-$ anion is 0.227 Å. Because of the rigidity of the macrocyclic tetradentate ligand, limited structural distortion occurs on formation of the reduced $3d^{10}$ $[\mathbf{1}]^-$ anion. As would be expected for this structure the rigid planar ligand and the strong electron donating amidate groups destabilize the copper (I) state, resulting in rapid dissociation, consistent with the highly negative and irreversible reduction potential. It is possible that the $3d^{10}$ copper(I) anion may adopt a five-coordinate structure where a solvent molecule is bound in an apical site, in a similar manner to the isoelectronic complexes **3** and **4**. The electrochemical results showed that reduction is rapidly followed by dissociations, and formation of a 5-coordinated species is a possible mechanism which facilitates demetalation.

Figure 6a shows the molecular orbital isosurface of the β-LUMO for complex **1**; the spatial counterpart of this orbital is the α-HOMO-2 orbital, in which the unpaired electron resides. This orbital displays in-plane σ-anti-bonding character between the Cu(II) center and the four nitrogen donor atoms. Figure S2 (Supporting Information) shows the spatial distribution of the frontier molecular orbitals (FMO) for the neutral copper(II) complex, **1** and the anionic copper(I) complex [**1**]$^{-}$. The calculated Mulliken spin density isosurface (99%) (Figure 6b) for complex **1** shows that the unpaired electron is mainly located on the copper(II) ion which has a Mulliken spin density of 0.493. The two donor nitrogen atoms N1 and N4 have a residual spin density of 0.170, and the N2/N3 donor atoms have a spin density of 0.070. As expected in C_s symmetry, the calculations predict that the four donor nitrogen atoms will couple to the unpaired electron centered on the metal ion to give two different superhyperfine coupling constants in the EPR spectrum.

The DFT calculations predict that upon oxidation of complex **1**, the diradical [**1**$^{\bullet}$]$^{+}$ triplet will be more stable than the singlet, copper(III) complex [**1**]$^{+}$. Formation of the triplet species requires removal of an electron from the ligand-based β-HOMO (Figure S3, Supporting Information). For the triplet [**1**$^{\bullet}$]$^{+}$ species, the rmsd between the structure of the optimized copper(II) complex **1** and the cationic species is 0.302 Å, while that between the X-ray crystal structure of **1** and [**1**$^{\bullet}$]$^{+}$ is 0.298 Å. It is possible that for the diradical [**1**$^{\bullet}$]$^{+}$ triplet state, antiferromagnetic coupling of the two unpaired electrons occupying predominantly metal- and ligand-based molecular orbitals may generate a singlet diradical species. However, this singlet diradical has not been calculated.

To interpret the results of the SEC experiments time-dependent density functional theory (TD-DFT) calculations were used to simulate the electronic absorption spectra of complex **1** and [**1**$^{\bullet}$]$^{+}$ (Figure 4b), and predict the nature of the excited states and electronic transitions involved. The simulated spectra show peaks at 420 nm (f_{calc} = 0.0137) and 412 nm (f_{calc} = 0.0686) for **1** and the triplet [**1**$^{\bullet}$]$^{+}$, respectively. In the case of the neutral complex **1** the calculated transition that gives rise to the band at 420 nm is assigned mainly to the redistribution of electron density between metal centered d orbitals. While for the [**1**$^{\bullet}$]$^{+}$ triplet the band at 412 nm is assigned mainly to the reorganization of the electron density in the $\pi\pi^*$ orbitals of the benzyl and amide carbonyl components of the ligand. This is in very good agreement with the experimental spectra. In both spectra, two major bands are predicted with one band in the visible region and one more intense band in the UV. The calculations correctly predict the increase in intensity of the visible band on oxidation. The differences in oscillator strengths and calculated band energies between the TD-DFT simulated spectra and the experimental data are likely due to the absence of solvation effects in the calculations.

Radiochemistry

The ligand H_2**L** has been investigated as a potential chelating agent for ^{64}Cu. Two strategies were used for the synthesis of ^{64}Cu labeled complexes of H_2**L**. The first (Scheme 3, A) involved direct labeling of the pro-ligand with ^{64}Cu(II) (a solution of ^{64}Cu(OAc)$_2$ and H_2**L** (pH 8) were heated at 40 °C for 1 h). The second approach (Scheme 3, B) involved transmetalation of complex **3** with the radiometal to give the radiolabeled complex, (the pH

of a solution containing $^{64}Cu(OAc)_2$ and **3** was adjusted to pH 10 with NaOH and the mixture stirred at RT for 10 min). Figure 7 shows the radio-HPLC chromatograms for ^{64}Cu-**1** prepared via transmetalation from complex **3**. Identical retention times were observed for the complexes when prepared from the pro-ligand or the Zn(II) precursor complex. The radiochemical purity of the ^{64}Cu species was estimated by integration from the radio-HPLC chromatograms to be 95%. Basic conditions were required for labeling ^{64}Cu to ensure deprotonation of the amide groups.

As discussed previously the non-radioactive Ga(III) complex of the deprotonated form of H_2**L** has been prepared and ^{68}Ga- and ^{99m}Tc-labeling studies will be conducted in due course.

Biodistribution

Biodistribution data at 1, 2, 4, and 24 h post-intravenous tail vein injection of ^{64}Cu-**1** in male Lewis rats are shown in Figure 8. The majority of the activity cleared from the blood within 1 h post-administration (0.52 ± 0.12%ID/organ). The blood concentration then decreased slowly out to 24 h (0.30 ± 0.06%ID/organ at 24 h), suggesting that a small fraction of the administered ^{64}Cu remains associated with, for example, serum proteins. In comparison, ^{64}Cu-CB-TE2A, (CB-TE2A = 4,1-bis(carboxymethyl)-1,4,8,11-tetraazabicyclo[6.6.2]hexadecane) which is stable with respect to ligand dissociation, shows an approximately 10-fold more rapid blood clearance rate than ^{64}Cu-**1** with 0.032 ± 0.014%ID/organ remaining in the blood after 1 h.[35] The relatively fast excretion time of ^{64}Cu-**1** may result from either rapid clearance of the intact complex or fast metabolism of the complex followed by excretion of the metabolite. The complex appears to clear through the gastrointestinal tract via the liver. Low but significant levels of liver uptake were observed with 1.73 ± 0.38%ID/organ at 1 h, and this level did not vary greatly even after 24 h post-injection (0.97 ± 0.22%ID/organ at 24 h). For ^{64}Cu-CB-TE2A, liver uptake in rats was 0.14 ± 0.03%ID/organ at 24 h.[37] At the first time point the majority of ^{64}Cu-activity was found in the upper large intestine (14.35 ± 2.13%ID/organ at 1 h), and at 4 h this activity was found in the lower large intestine (15.46 ± 0.70%ID/organ at 4 h), which then decreased greatly by 24 h (3.25 ± 2.79%ID/organ at 24 h). No significant brain or heart uptake was observed (0.013 ± 0.007%ID/organ and 0.019 ± 0.02%ID/organ at 1 h, respectively). These biodistribution studies suggest that the complex ^{64}Cu-**1** with further functionalization at, for example, the benzene ring, has the potential to be used as the basis of a new chelator for conjugation to peptides and macromolecules.

Conclusion

The coordination chemistry of the N_4-macrocyclic ligand 2,10-dioxo-1,4,8,11-tetraazabicyclo[11.4.0]1,12-heptadeca-1 (12),14,16-triene H_2**L** has been investigated with the metal ions Cu(II), Ni(II), Zn(II), and Ga(III). In each case coordination of the macrocycle to the metal center occurs via the two amine nitrogen donors and two deprotonated amide nitrogen donors. X-ray structural studies show that the Cu(II) and Ni(II) complexes adopt four-coordinate, slightly distorted square-planar geometries while the d^{10} ions Zn(II) and Ga(III) are five coordinate with a molecule of water or a chloride ion in the

apical positions respectively. Electrochemical studies on complex **1** show that this complex is reversibly oxidized with $E_{1/2}$ = 0.47 V and irreversibly reduced at E_P = −1.84 V. The oxidized counterpart of complex **1** was generated in situ by electrochemical oxidation using an optically transparent thin-layer electrochemical (OTTLE) cell. TD-DFT calculations were used to simulate the electronic absorption spectrum of the oxidized species and indicate that oxidation involves removal of an electron from the ligand to give a radical cation as opposed to oxidation at the metal center yielding a singlet species. DFT calculations also accurately reproduced the geometries of the four complexes. The ligand has been radiolabeled with ^{64}Cu(II). Radiolabeling was achieved by either direct labeling of the ligand or via transmetalation of the preformed Zn(II) complex. The biodistribution of the ^{64}Cu labeled complex has been investigated in male Lewis rats and showed that the complex cleared rapidly from the blood out to 1–2 h post-injection.

Experimental Section

General Procedures

All reagents and solvents were obtained from commercial sources (Sigma-Aldrich, Lancaster and Alfa Aesar) and unless otherwise stated were used as received. Elemental analyses were performed by the microanalysis service of the Department of Inorganic Chemistry at the University of Oxford. NMR spectra were recorded on a Varian Mercury VX300 spectrometer, (^{1}H at 300.17 MHz, ^{13}C at 75.50 MHz) or a Bruker AVII 500 with ^{13}C cryoprobe (^{1}H at 500.30 MHz, ^{13}C at 125.80 MHz) using the residual solvent signal as an internal reference. UV/vis spectra were recorded on a Perkin-Elmer Lambda 19 UV/vis/near-IR spectrometer. EPR spectra were recorded in a capillary tube using a Bruker EMX-micro X-band spectrometer. Electrochemistry experiments were performed using a CH Instruments Electrochemical Analyzer. The potentiostat was controlled by using a PC running CH Instruments version 2.05 electrochemical software. All cyclic voltammetry measurements were recorded in a glass cell sealed with a Teflon cap and located inside a Faraday cage at a temperature of 21.5 ± 1.5 °C. Complex solutions were prepared in anhydrous dimethyl formamide (DMF) with 0.1 M tetra-*n*-butylammonium tetrafluoroborate (Bu_4NBF_4) supporting electrolyte. All solutions were vigorously degassed for >15 min with dry nitrogen before each experiment, and measurements were recorded under a nitrogen atmosphere. An electronic positive feedback scheme was used to correct for the effect of uncompensated (ohmic drop, iR_u) resistance between the working and reference electrodes. Cyclic voltammograms were recorded in a three-electrode cell using a platinum disk working electrode (1.0 mm diameter) at scan rates between 0.02 and 1.00 V s^{-1}. A platinum wire counter/auxiliary electrode and a silver/silver ion reference electrode (BAS) were used. Ferrocene was used as an internal reference for which the one-electron redox process occurs at $E_{1/2}$ = + 0.53 V (DMF) versus SCE.

UV/vis SEC experiments were performed in anhydrous DMF with 0.1 M Bu_4NBF_4 supporting electrolyte, using a custom-made optically transparent thin-layer electrode (OTTLE) quartz cell (path length, l = 0.46 mm), sealed with a Teflon cap. The total volume of the OTTLE cell was approximately 4 mL. The same auxiliary and reference electrodes as used in the cyclic voltammetry were situated in the bulk solution above the cavity, and a

platinum wire mesh (approximately 50-wires per inch, 0.10 mm thickness) located inside the cavity was used as the working electrode.

X-ray Crystallography

Single crystals of **1**–**4** suitable for X-ray diffraction studies were grown by slow evaporation of methanol solutions of each compound. Crystallographic data for all structures determined are given in Table 1 Crystals were mounted on a glass fiber and cooled rapidly to 150 K in a stream of cold N_2 by using an Oxford Cryosystems CRYOSTREAM unit. Diffraction data were measured by using an Enraf–Nonius Kappa CCD diffractometer (graphite-monochromated Mo Kα radiation, λ = 0.71073 Å). Cell parameters and intensities were corrected for absorption effects by using the multiscan method based on multiple scans of identical reflections, and intensity data were processed by using the DENZO-SMN package.[36] Space groups were identified by examination of the systematic absences in the intensity data. The structures were solved by using the direct methods program SIR92,[37] which located all non-hydrogen atoms. Subsequent full-matrix least-squares refinement was carried out by using the CRYSTALS program suite.[38] Coordinates and anisotropic thermal parameters of all non-hydrogen atoms were refined. The NH hydrogen atoms were located in the difference Fourier map, and their coordinates and isotropic thermal parameters were subsequently refined. Other hydrogen atoms were positioned geometrically after each cycle of refinement. A three-term Chebychev polynomial weighting scheme was applied. Images were generated by using ORTEP-3.[32] CCDC-717613 (for **1**), −717614 (for **2**), −717615 (for **4**), and −717616 (for **3**) contain the supplementary crystallographic data for this paper. This data can be obtained free of charge from The Cambridge Crystallographic Data Centre via www.ccdc.cam.ac.uk/data_request/cif.

Density Functional Calculations

All calculations were conducted using density functional theory (DFT) as implemented in the Gaussian 03 suite of ab initio quantum chemistry programs. Geometry optimizations and vibrational frequency calculations were performed by using the hybrid-DFT B3LYP exchange-correlation functionals and the double-ζ6–31 + + G(d,p) basis set for all atoms. Normal self-consistent field (SCF) and geometry convergence criteria were employed throughout using either C_S or C_1 symmetry. For all gas phase calculations, harmonic frequency analysis based on analytical second derivates was used to characterize the optimized geometries as local minima and to derive the zero-point energy (ZPE) and vibrational/rotational/translational contributions to the enthalpic and entropic corrections at standard temperature and pressure (298.15 K and 1.000 atm respectively). Unscaled frequencies were used for the vibrational component to the entropy.

The effects of solvation were incorporated iteratively by performing self-consistent reaction field (SCRF) calculations using the integral equation formalism polarizable continuum model (IEFPCM) initially developed by Tomasi and co-workers. [39] The solute–solvent boundary has been defined using a solvent excluding surface (SES) with a molecular surface defined using the United Atom Topological model (UAHF) for the radii of the solute atoms. Two solvent models were employed; water (ε = 78.39, R_{solv} = 1.385 Å) and DMF(ε = 36.7, R_{solv} = 2.67 Å) where ε is the dielectric constant and R_{solv} is the sphere radius of the solvent.

Geometry optimizations were performed in the presence of the reaction field using the optimized gas phase coordinates as initial geometries. In this dielectric continuum model, the solute is placed in a cavity within the solvent continuum. Vertical transition energies and oscillator strengths for electronic excitation to the first 24 singlet excited states of the neutral copper(II) species, **1**, and the cationic triplet $[\mathbf{1}^{\bullet}]^{+}$ species were calculated using TD-DFT and the unrestricted uB3LYP/6–31 + + G(d,p) methodology. The geometries used were obtained from the ground-state optimizations at the same level of theory. Calculations were performed using C_s symmetry. Electronic absorption spectra were simulated using the SWizard program as a convolution of Gaussian-shaped bands fit over the energies and oscillator strengths of the calculated excited states. Qualitatively, the best simulated spectra were calculated using a half-bandwidth, $\Delta_{1/2}$, of 3500 cm^{-1} for each calculated transition.

Synthesis

N,*N*′-bis(chloroacetyl)-1,2-phenylenediamine: To an ice cold mixture of 1,2-phenylenediamine (15.14 g, 140 mM) and K_2CO_3 (37.3 g, 270 mmol) in dichloromethane (150 mL) was added dropwise a solution of chloroacetyl chloride (21.5 mL, 270 mmol) in dichloromethane (50 mL) over a period of 2 h. The mixture was allowed to warm to room temperature (RT) and stirred overnight. The insoluble material was collected by vacuum filtration and resuspended in water (300 mL), and the mixture stirred for 0.5 h. The crude product was recollected by vacuum filtration and washed with water (2 × 50 mL), air-dried, and recrystallized from acetonitrile (400 mL). Yield of gray crystalline solid (12.41 g, 34.0%). Found: C, 46.2; H, 3.9; N, 10.8%. $C_{10}H_{10}N_2O_2Cl_2$ requires C, 46.0; H, 3.8; N, 10.7%.

H_2L—To a mixture of *N*,*N*′-bis(chloroacetyl)-1,2-phenylenediamine (6.0 g, 23 mmol) and Na_2CO_3 (24.4 g, 230 mmol) in acetonitrile heated to 70 °C was added a solution of 1,3-diaminopropane (1.9 mL, 23 mmol) in acetonitrile (50 mL). The mixture was refluxed at 90 °C for 12 h, and then the hot solution was filtered through a fluted filter paper and the filtrate taken to dryness under reduced pressure. The resultant crude product was recrystallized from acetonitrile. Yield of cream colored crystalline solid (2.98 g, 49.4%). Found: C, 59.5; H, 6.9; N, 21.3%. $C_{13}H_{18}N_4O_2$ requires C, 59.5; H, 6.9; N, 21.4%. ^{1}H NMR (500.30 MHz, $(CD_3)_2SO$) δ = 7.78–7.72, 7.16–7.10 (m, 4H, ArH), 3.20 (4H, s, $COCH_2$), 2.77 (t, $^3J_{HH}$ 5.3 Hz, $(CH_2)_2CH_2$), 1.63 (quin, $^3J_{HH}$ 5.5 Hz, $(CH_2)_2CH_2$). ^{13}C NMR (125.81 MHz, $(CD_3)_2SO$) δ = 169.82 (C=O), 128.86 (ArC), 124.21 (ArCH), 122.86 (ArCH), 52.79 ($COCH_2$), 45.38 ($(CH_2)_2CH_2$), 29.54 ($(CH_2)_2CH_2$).

1: To a mixture of H_2**L** (200 mg, 0.76 mmol) and $CuCl_2{\cdot}2H_2O$ (130 mg, 0.76 mmol) in methanol (75 mL) heated to 60 °C was added sodium methoxide (124 mg, 2.3 mmol). The resultant mixture was heated at reflux for 1 h during which time a deep red precipitate formed. The crude product was collected at the pump and recrystallized from a mixture of 1:1 methanol/water (150 mL). Yield of crystalline red solid (169 mg, 68.3%). Found: C, 45.5; H, 5.4; N, 16.3%. $CuC_{13}H_{16}N_4O_2{\cdot}H_2O$ requires C, 45.7; H, 5.3; N, 16.4%.

2: Prepared using the same procedure as described for **1** from H_2**L** (500 mg, 1.9 mmol), $NiCl_2{\cdot}6H_2O$ (453 mg, 1.9 mmol), sodium methoxide (310 mg, 5.7 mmol), and methanol

(150 mL). Yield of crystalline yellow solid (283 mg, 46.4%). Found: C, 47.8; H, 5.4; N, 17.0%. $NiC_{13}H_{16}N_4O_2 \cdot 0.5H_2O$ requires C, 47.6; H, 5.2; N, 17.1%. ^{1}H NMR (500.30 MHz, $(CD_3)_2SO$) δ = 7.96–7.93, 6.59–6.56 (4H, m, ArH), 4.49 (2H, m, NH), 3.24 (2H, dd, $^2J_{HH}$ 16.4 Hz, $^3J_{HH}$ 6.9 Hz, $COCH_2$), 3.15 (2H, dd, $^2J_{HH}$ 16.4 Hz, $^3J_{HH}$ 6.9 Hz, $COCH_2$), 2.71 (2H, m, $(CH_2)_2CH_2$), 2.48 (2H, m, $(CH_2)_2CH_2$), 1.68 (1H, dt, $^2J_{HH}$ 15.5 Hz, $^3J_{HH}$ 5.0 Hz, $(CH_2)_2CH_2$), 1.06 (1H, dtt, $^2J_{HH}$ 15.5 Hz, $^3J_{HH}$ 14.8 Hz, $^3J_{HH}$ 5.0 Hz, $(CH_2)_2CH_2$). ^{13}C NMR (125.81 MHz, $(CD_3)_2SO$) δ = 173.23 (C=O), 142.50 (ArC), 120.28 (ArCH), 118.27 (ArCH), 59.23 ($COCH_2$), 49.16 ($(CH_2)_2CH_2$), 26.87 ($(CH_2)_2CH_2$).

3: Prepared using the same procedure as described for **1** from H_2**L** (500 mg, 1.9 mmol), $ZnCl_2$ (260 mg, 1.9 mmol), sodium methoxide (310 mg, 5.7 mmol), and methanol (150 mL). Yield of white powder (131 mg, 21.2%). Found: C, 43.1; H, 5.5; N, 15.4%. $ZnC_{13}H_{16}N_4O_2 \cdot 2H_2O$ requires C, 43.2; H, 5.6; N, 15.5%. ^{1}H NMR (500.30 MHz, $(CD_3)_2SO$) δ = 8.13–8.10, 6.66–6.62 (4H, m, ArH), 4.49 (2H, m, NH), 3.31 (2H, m, $COCH_2$), 2.49 (2H, m, $COCH_2$), 2.85 (2H, a, $^2J_{HH}$ 11.6 Hz, $(CH_2)_2CH_2$), 2.36 (2H, dd, $^2J_{HH}$ 11.9 Hz, $^3J_{HH}$ 11.6 Hz, $(CH_2)_2CH_2$), 1.66 (2H, m, $(CH_2)_2CH_2$). ^{13}C NMR (125.81 MHz, $(CD_3)_2SO$) δ = 168.29 (C=O), 139.36 (ArC), 120.24 (ArCH), 120.08 (ArCH), 56.02 ($COCH_2$), 42.24 ($(CH_2)_2CH_2$), 28.52 ($(CH_2)_2CH_2$).

4: Prepared using the same procedure as described for **1** from H_2**L** (400 mg, 1.9 mmol), $GaCl_3$ (269 mg, 1.5 mmol), sodium methoxide (247 mg, 4.6 mmol), and methanol (110 mL). Yield of white microcrystalline powder (297 mg, 53.2%). Found: C, 40.0; H, 4.9; N, 14.4%. $GaC_{13}H_{16}N_4O_2 \cdot 1.5H_2O$ requires C, 39.8; H, 4.9; N, 14.4%. ^{1}H NMR (500.30 MHz, $(CD_3)_2SO$) δ = 8.21–8.17, 6.87–6.84 (4H, m, ArH), 6.38 (2H, m, NH), 3.57 (2H, dd, $^2J_{HH}$ 15.9 Hz, $^3J_{HH}$ 5.6 Hz, $COCH_2$), 2.89 (2H, m, $COCH_2$), 3.02 (2H, d, $^2J_{HH}$ 10.5 Hz, $(CH_2)_2CH_2$), 2.89 (2H, m, $(CH_2)_2CH_2$), 1.92 (1H, dtt, $^2J_{HH}$ 15.5 Hz, $^3J_{HH}$ 12.6 Hz, $^3J_{HH}$ 2.2 Hz, $(CH_2)_2CH_2$), 1.83 (1H, dt, $^2J_{HH}$ 15.5 Hz, $^3J_{HH}$ 2.2 Hz, $(CH_2)_2CH_2$). ^{13}C NMR (125.81 MHz, $(CD_3)_2SO$) δ = 166.13 (C=O), 134.10 (ArC), 121.46 (ArCH), 117.69 (ArCH), 53.58 ($COCH_2$), 50.67 ($(CH_2)_2CH_2$), 26.11 ($(CH_2)_2CH_2$).

Radiochemistry. Using Pro-Ligand

^{64}Cu-1—The copper-64 labeled complex, ^{64}Cu-**1**, was prepared by adding an aqueous solution of approximately 37 MBq of $^{64}Cu(OAc)_2$ (0.1 mL; pH 8.0) to a DMSO/H_2O solution (1:9; 0.45 mL) of H_2**L** (1 mg/mL). The resultant mixture was shaken at 40 °C for 1 h. The complex, ^{64}Cu-**1** had an R_f of 0.76 as observed by radio-TLC using C18 plates and an eluent mixture of 10% NH_4OAc/MeOH (70:30 v/v). Radio HPLC analysis corroborated the TLC results. Both methods demonstrated that the complex showed a radiochemical purity greater than 95%.

Transmetalation

^{64}Cu-1—A solution of $^{64}Cu(OAc)_2$ (34 μL ~10 MBq) was added to a solution of **3** in methanol (100 μL of 1 mgmL^{-1}) and of NaOH (20 μL 1.0 M), and the solution was stirred at room temperature for 10 min.

Biodistribution

Biodistribution studies were performed in male Lewis rats with each rat receiving approximately 1.48 MBq (150 uL) of ^{64}Cu-**1** diluted in 0.9% saline. Animals were sacrificed at selected time points post-injection (p.i.), and the organs of interest were removed, weighed, and the radioactivity was counted on a Beckman Gamma Counter 8000. The percent injected dose per gram (%ID/gram) and percent injected dose per organ (%ID/organ) were calculated by comparison to a weighed, counted standard.

Supplementary Material

Refer to Web version on PubMed Central for supplementary material.

Acknowledgments

P.J.B. thanks GlaxoSmithKline for a fellowship and we are grateful to Dr. A. Gee for helpful discussions. J.P.H. thanks Merton College and the EPSRC for funding. S.R.B. thanks DTI and Siemens Molecular Imaging Ltd for a fellowship. We thank the Oxford Supercomputing Centre for assistance with the DFT calculations. We also acknowledge Grants F32 CA115148 (T.J.W.) and R24 CA86307 (production of ^{64}Cu and Washington University School of Medicine).

References

1. Bayly SR, Christlieb M, Barnard PJ, Betts HM, Holland JP, Hueting R, King RC, Aigbirhio FI, Dilworth JR, Honess DJ, Wardman P. J Nucl Med. 2008; 49(11):1862–1868. [PubMed: 18927340]
2. Holland JP, Barnard PJ, Collison D, Dilworth JR, Edge R, Green JC, McInnes EJL. Chem, Eur J. 2008; 14(19):5890–5907. [PubMed: 18494010]
3. Holland JP, Aigbirhio FI, Betts HM, Bonnitcha PD, Burke P, Christlieb M, Churchill GC, Cowley AR, Dilworth JR, Donnelly PS, Green JC, Peach JM, Vasudevan SR, Warren JE. Inorg Chem. 2007; 46(2):465–485. [PubMed: 17279826]
4. Betts HM, Barnard PJ, Bayly SR, Dilworth JR, Gee AD, Holland JP. Angew Chem, Int Ed. 2008; 47:8416–8419.
5. Fujibayashi Y, Taniuchi H, Yonekura Y, Ohtani H, Konishi J, Yokoyama A. J Nucl Med. 1997; 38(7):1155–1160. [PubMed: 9225812]
6. Obata A, Yoshimi E, Waki A, Lewis JS, Oyama N, Welch MJ, Saji H, Yonekura Y, Fujibayashi Y. Ann Nucl Med. 2001; 15(6):499–504. [PubMed: 11831397]
7. Dearling JLJ, Lewis JS, McCarthy DW, Welch MJ, Blower PJ. Chem Commun. 1998; 22:2531–2532.
8. Dearling JLJ, Lewis JS, Mullen GED, Welch MJ, Blower PJ. J Biol Inorg Chem. 2002; 7(3):249–259. [PubMed: 11935349]
9. Maurer RI, Blower PJ, Dilworth JR, Reynolds CA, Zheng Y, Mullen GED. J Med Chem. 2002; 45(7):1420–1431. [PubMed: 11906283]
10. Holland JP, Green JC, Dilworth JR. Dalton Trans. 2006; 6:783–794. [PubMed: 16437173]
11. Xiao Z, Donnelly PS, Zimmermann M, Wedd AG. Inorg Chem. 2008; 47(10):4338–4347. [PubMed: 18412332]
12. Smith SV. J Inorg Biochem. 2004; 98(11):1874–1901. [PubMed: 15522415]
13. Anderson CJ, Welch MJ. Chem Rev. 1999; 99(9):2219–2234. [PubMed: 11749480]
14. Sun XK, Wuest M, Kovacs Z, Sherry AD, Motekaitis R, Wang Z, Martell AE, Welch MJ, Anderson CJ. J Biol Inorg Chem. 2003; 8(1–2):217–225. [PubMed: 12459917]
15. Bass LA, Wang M, Welch MJ, Anderson CJ. Bioconjugate Chem. 2000; 11(4):527–532.
16. Boswell CA, Sun X, Niu W, Weisman GR, Wong EH, Rheingold AL, Anderson CJ. J Med Chem. 2004; 47(6):1465–1474. [PubMed: 14998334]

17. Woodin KS, Heroux KJ, Boswell CA, Wong EH, Weisman GR, Niu W, Tomellini SA, Anderson CJ, Zakharov LN, Rheingold AL. Eur J Inorg Chem. 2005; (23):4829–4833.
18. Margerum DW, Chellappa KL, Bossu FP, Burce GL. J Am Chem Soc. 1975; 97(23):6894–6896. [PubMed: 1184889]
19. Bossu FP, Margerum DW. J Am Chem Soc. 1976; 98(13):4003–4004. [PubMed: 932353]
20. Kirksey ST Jr, Neubecker TA, Margerum DW. J Am Chem Soc. 1979; 101(6):1631–1633.
21. Diaddario LL, Robinson WR, Margerum DW. Inorg Chem. 1983; 22(7):1021–1025.
22. Collins TJ, Richmond TG, Santarsiero BD, Treco BGRT. J Am Chem Soc. 1986; 108(8):2088–2090.
23. Anson FC, Collins TJ, Richmond TG, Santarsiero BD, Toth JE, Treco BGRT. J Am Chem Soc. 1987; 109(10):2974–2979.
24. Collins TJ, Slebodnick C, Uffelman ES. Inorg Chem. 1990; 29(18):3433–3436.
25. Collins TJ, Kostka KL, Munck E, Uffelman ES. J Am Chem Soc. 1990; 112(14):5637–5639.
26. Bradshaw JS, Krakowiak KE, An A, Izatt RM. J Heterocyclic Chem. 1990; 27:2113–2116.
27. Antunes P, Delgado R, Drew MGB, Felix V, Maecke H. Inorg Chem. 2007; 46(8):3144–3153. [PubMed: 17378553]
28. Cutler CS, Wuest M, Anderson CJ, Reichert DE, Sun Y, Martell AE, Welch MJ. Nucl Med Biol. 2000; 27:375–380. [PubMed: 10938473]
29. Motekaitis RJ, Sun Y, Martell AE, Welch MJ. Can J Chem. 1999; 77:614–623.
30. Sigel H, Martin RB. Chem Rev. 1982; 82:385–426.
31. Laurie, SH. Amino Acids Peptides and Proteins. In: Wilkinson, G., editor. Comprehensive Coordination Chemistry. Pergamon Press; Oxford: 1987. p. 739-776.
32. Farrugia LJ. J Appl Crystallogr. 1997; 30:565.
33. Stoll S, Schweiger A. J Magn Reson. 2006; 178:42–55. [PubMed: 16188474]
34. Koch, W.; Holthausen, MC. A Chemists Guide to Density Functional Theory. 2. Wiley-VCH; Weinheim, Germany: 2001.
35. Sun X, Wuest M, Weisman GR, Wong EH, Reed DP, Boswell CA, Motekaitis R, Martell AE, Welch MJ, Anderson CJ. J Med Chem. 2002; 45(2):469–477. [PubMed: 11784151]
36. Otwinowski Z, Minor W. Methods Enzymol. 1997; 276:307.
37. Altomare A, Cascarano G, Giacovazzo G, Guagliardi A, Burla MC, Polidori G, Camalli G. J Appl Crystallogr. 1994; 27:435.
38. Betteridge PW, Carruthers JR, Cooper RI, Prout K, Watkin DJ. J Appl Crystallogr. 2003; 36:1487.
39. Tomasi J, Mennucci B, Cammi R. Chem Rev. 2005; 105(8):2999–3094. [PubMed: 16092826]

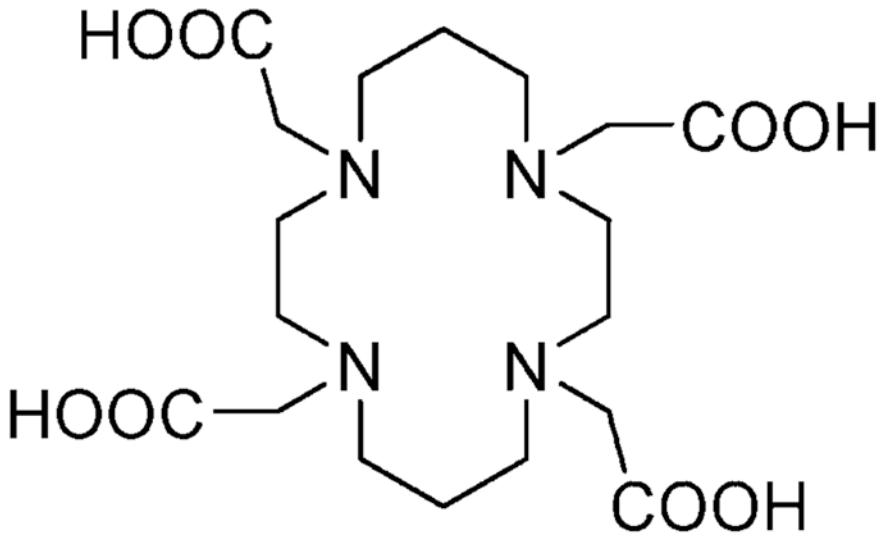

Figure 1.
Structure of the 14-membered macrocycle (cyclam) derivative TETA.

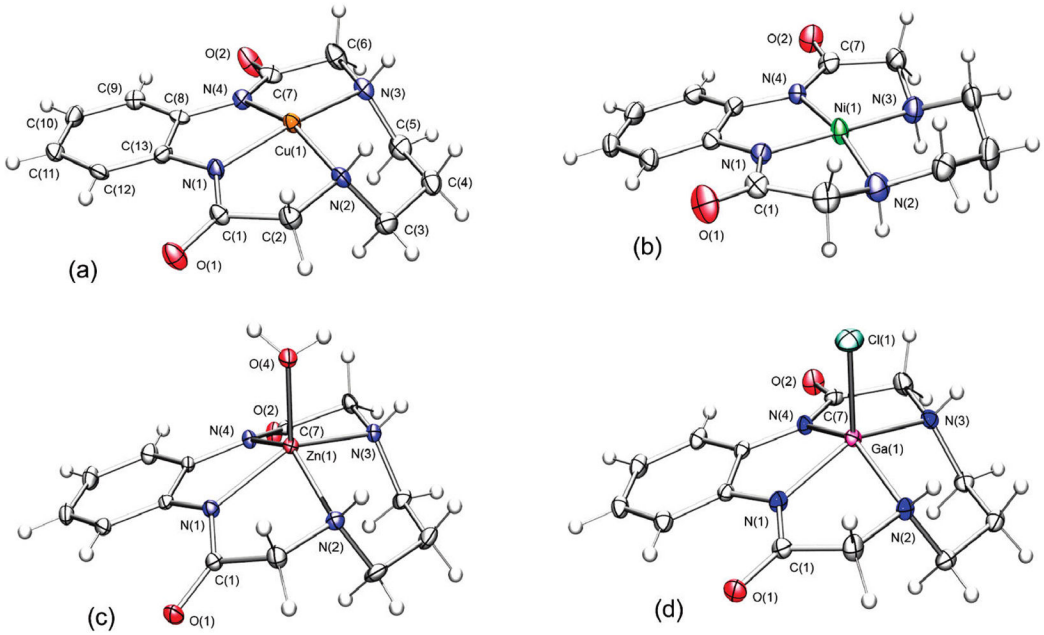

Figure 2.

ORTEP[32] representations of the molecular structures of complexes (a) **1**, (b) **2**, (c) **3**, and (d) **4**. The full ligand numbering scheme is given for **1** and the same scheme is used for **2–4**.

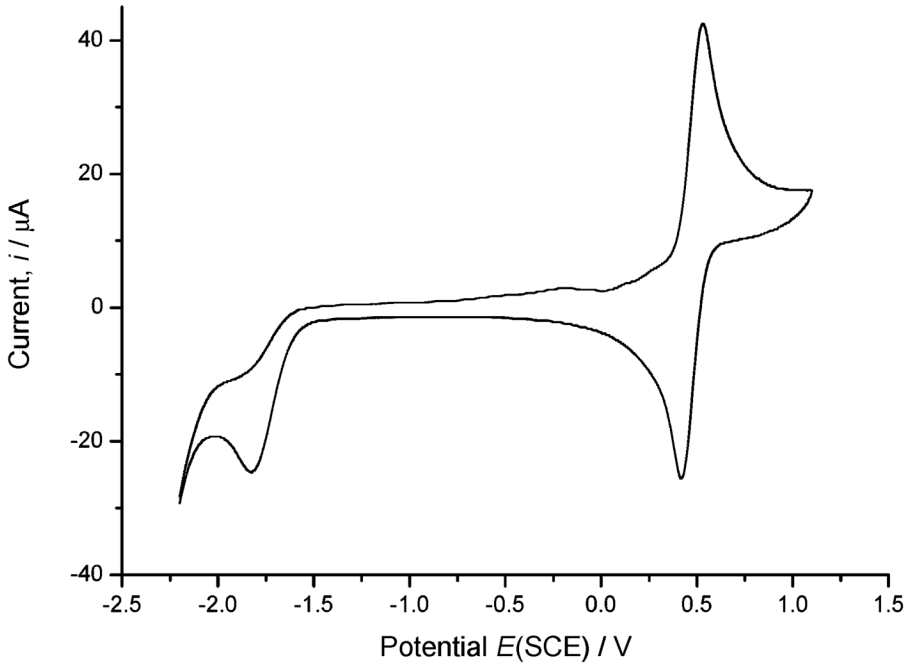

Figure 3.

Cyclic voltammogram of a solution of **1** (5.0×10^{-3} M, 22 °C) in anhydrous DMF recorded at 200 mV s^{-1} with $^{n}Bu_4NBF_4$ (0.10 M) supporting electrolyte recorded using a platinum disk electrode.

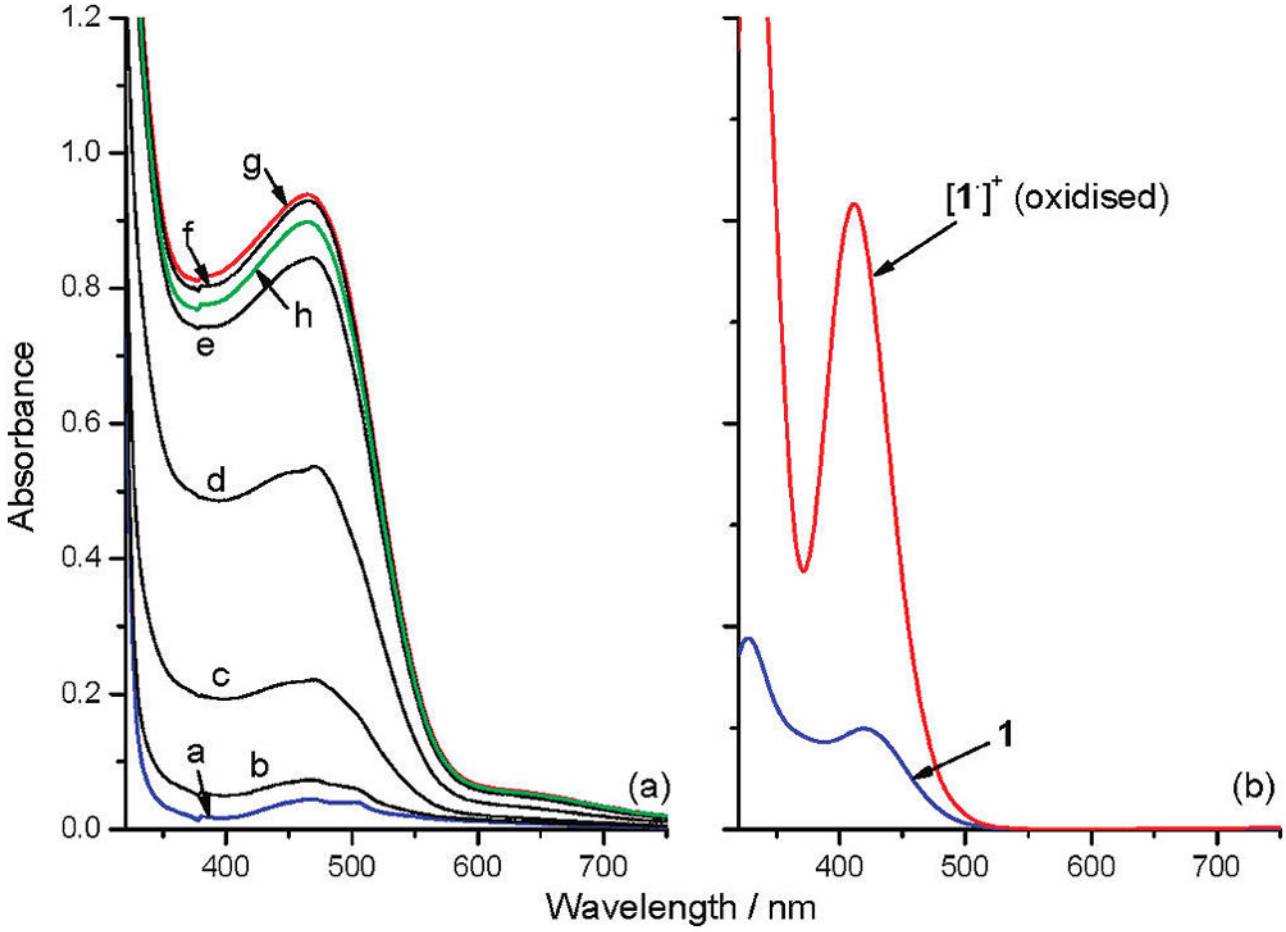

Figure 4.

(a) Change observed in the experimental UV/vis absorption spectrum after in situ electrochemical oxidation of a solution of **1** (1.0×10^{-3}M) in anhydrous, degassed DMF ($E_{appl.}$ = 1.13 V, *a* = 0 s, *b* = 40 s, *c* = 108 s, *d* = 212 s, *e* = 317 s, *f* = 420 s *g* = 733 s, *h* = 1200 s) and, (b) simulated TD-DFT electronic absorption spectra of the **1** (blue) and the cationic triplet species, $[\mathbf{1}^{\bullet}]^{+}$ (red).

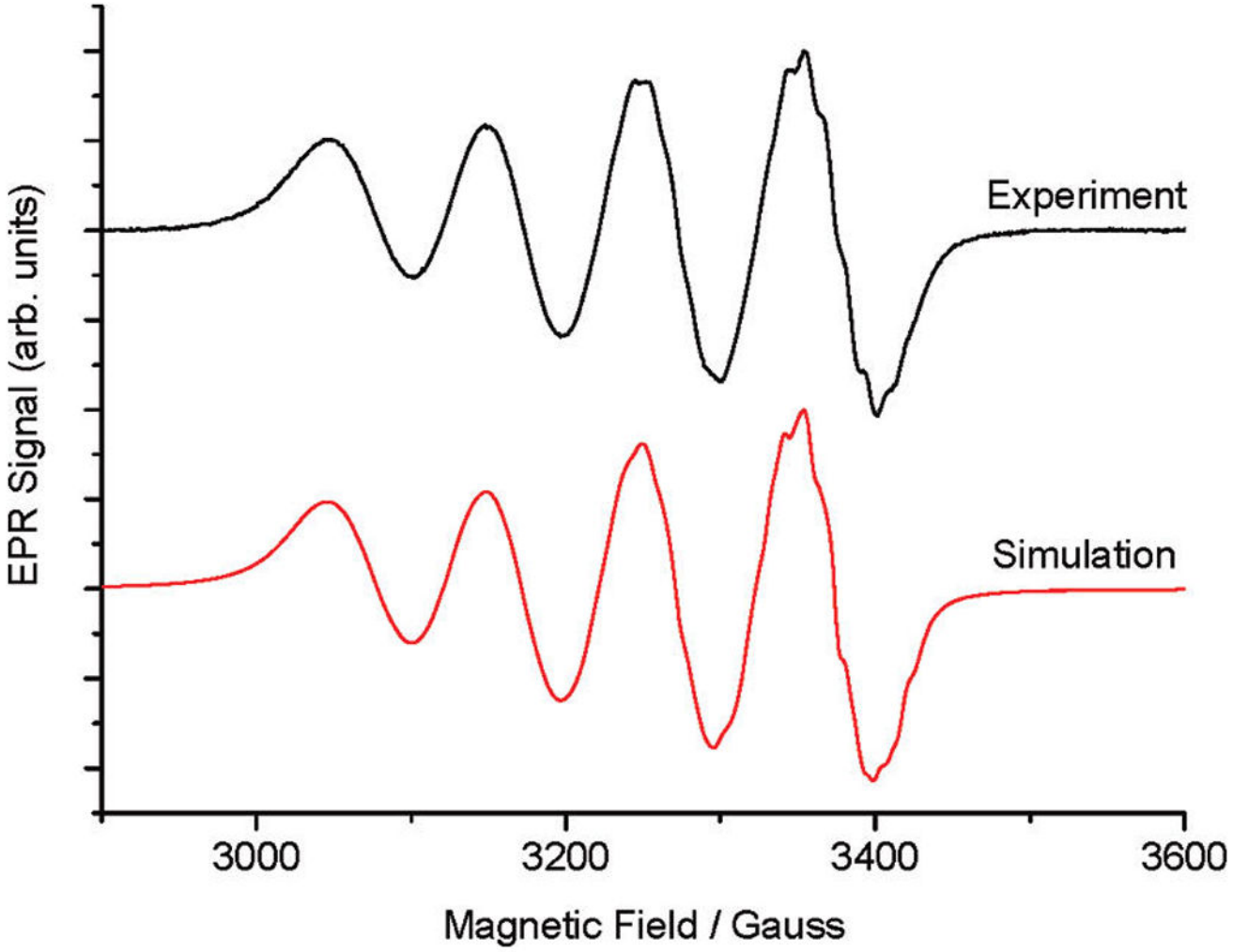

Figure 5.

Typical EPR spectrum (black) of a freshly prepared solution of **1** (5.0×10^{-3} M, 22 °C) in anhydrous DMF. The simulated spectrum (red) was performed using EasySpin.[33].

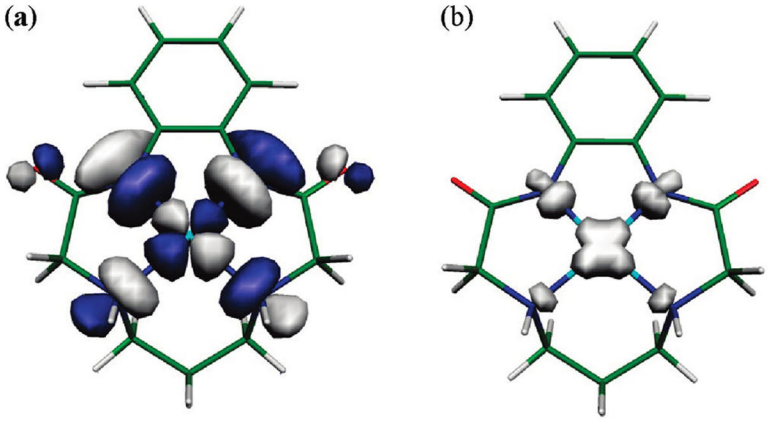

Figure 6.

(a) Spatial distribution of the unoccupied β-LUMO orbital of **1**. The α-spin spatial counterpart is the α-HOMO-2 orbital in which the unpaired electron resides, and this orbital electron density correlates with the location of the calculated Mulliken spin densities. (b) Isosurface representation of the total Mulliken spin density calculated by using the molecular orbital coefficients and mapped onto the optimized structure of **1**. In-plane delocalization of spin density on to the four nitrogen donor atoms can be seen.

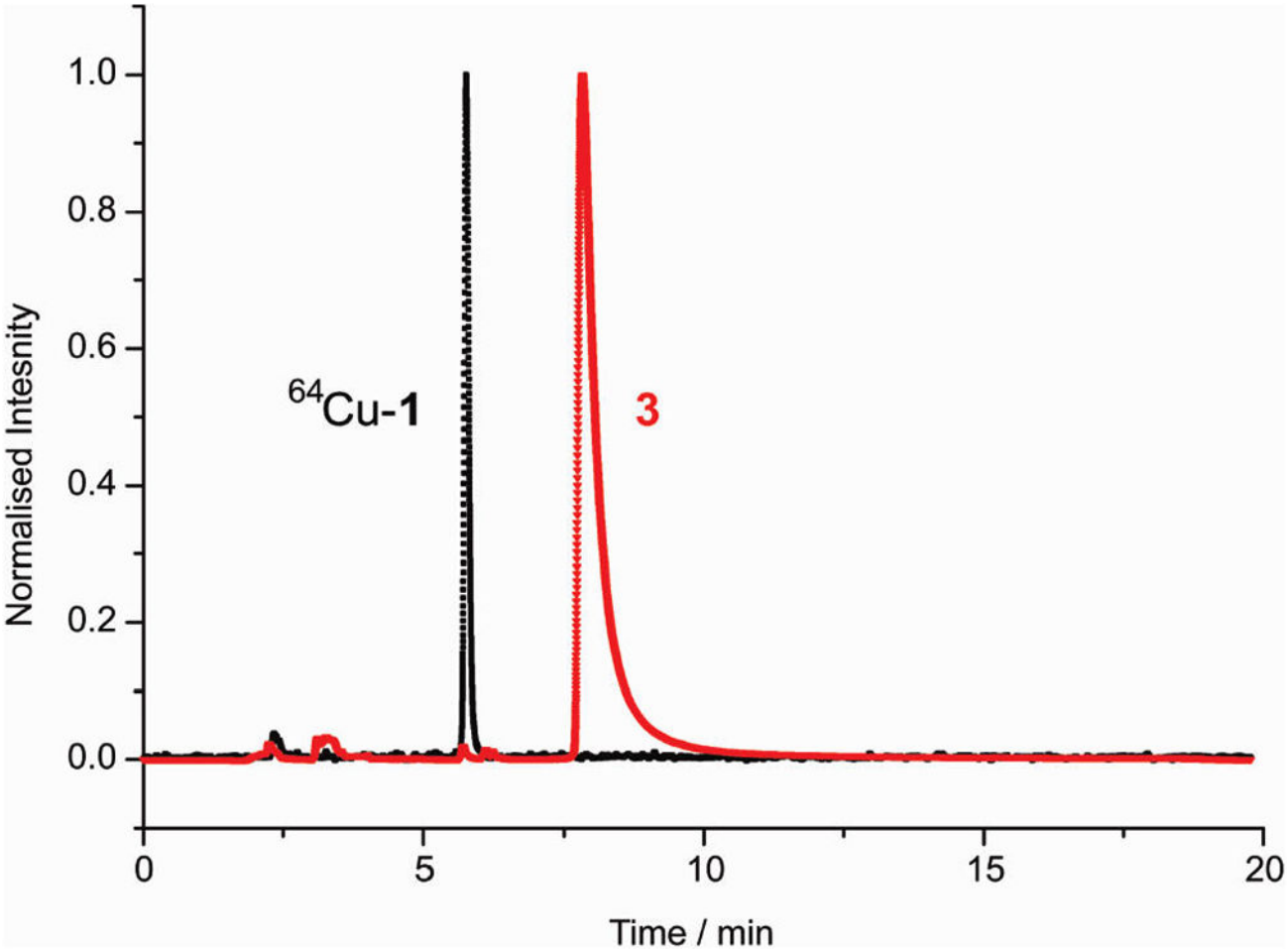

Figure 7.

Radio-HPLC chromatogram of the radiolabeled complex ^{64}Cu-**1** (black) prepared by transmetalation from **3** and the UV chromatogram of the precursor complex **3** (red).

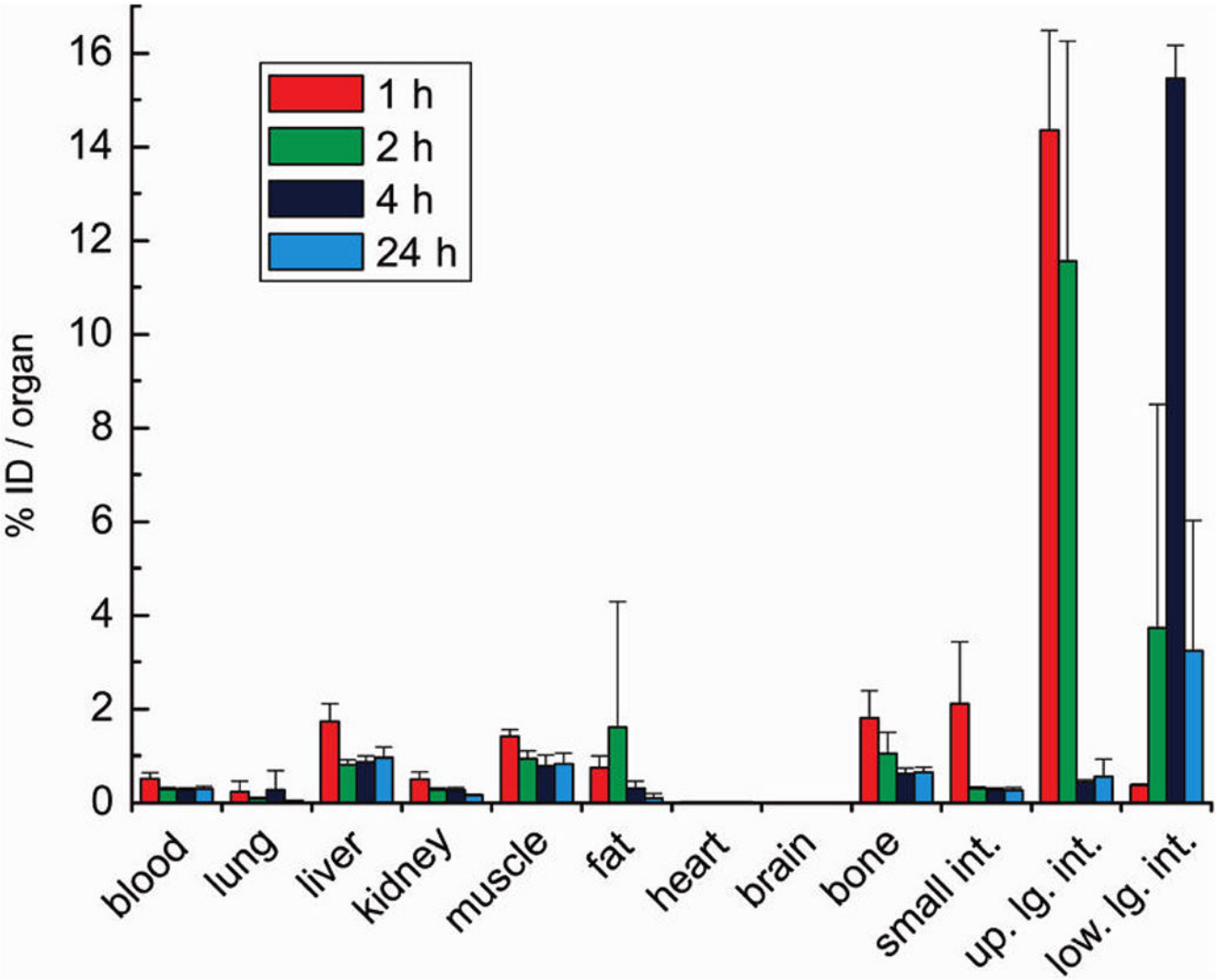

Figure 8.
Biodistribution of ^{64}Cu-**1** in normal male Lewis rats (n = 4 for each time point).

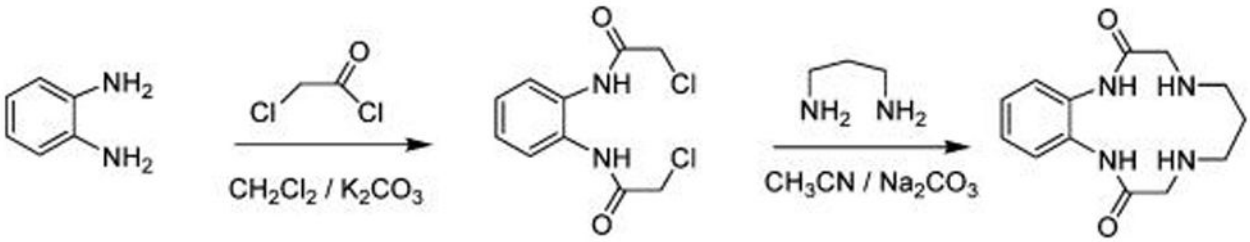

Scheme 1.
Synthesis of Macrocycle H_2**L**

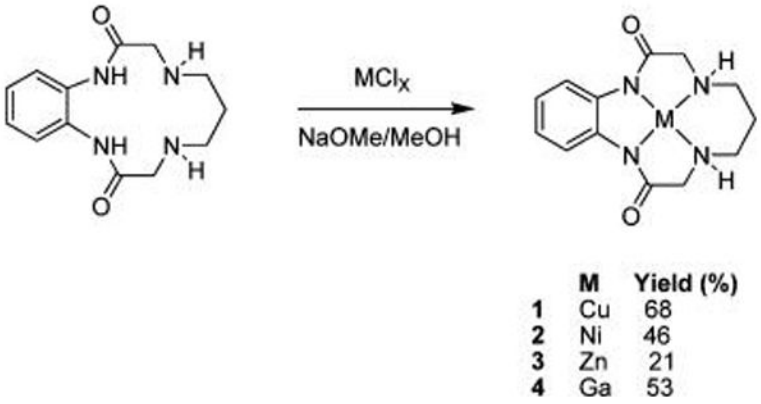

	M	Yield (%)
1	Cu	68
2	Ni	46
3	Zn	21
4	Ga	53

Scheme 2.
Metallation of H_2**L**

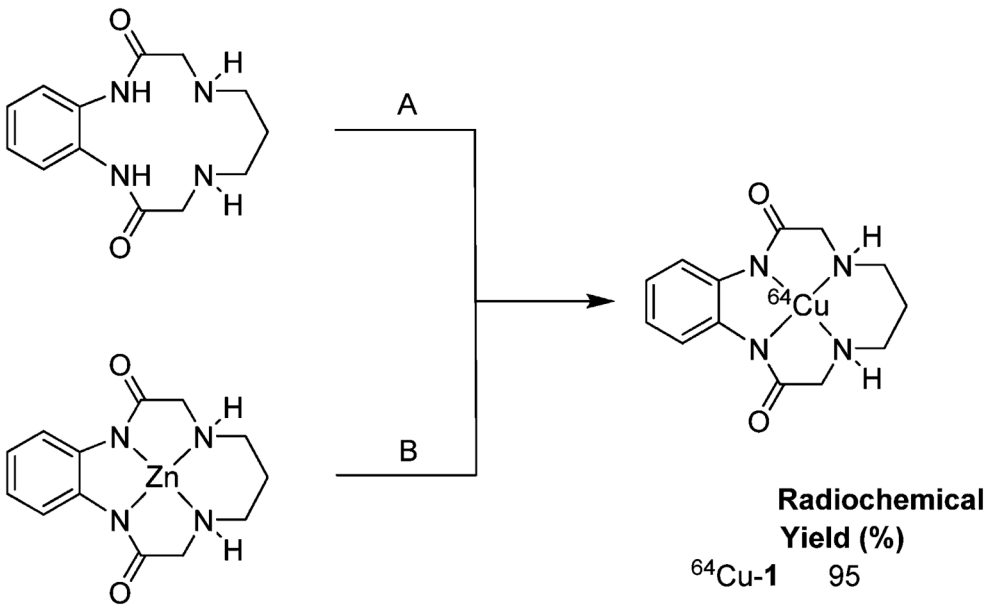

Scheme 3. Strategies Used for the Synthesis of Radiolabeled Complexes of the Ligand L[a]

[a] (A) Route from the pro-ligand. ^{64}Cu-**1**: $^{64}Cu(OAc)_2$ + H_2**L** (pH = 8). (B) Transmetallation from **3**. ^{64}Cu-**1: 3** + $^{64}Cu(OAc)_2$ + NaOH.

Table 1

Crystallographic Data for the Complexes **2**, **3**, and **4**

complex	**2**	**3**	**4**
chemical formula	$C_{13}H_{18}N_4NiO_3$	$C_{13}H_{20}N_4O_4Zn$	$C_{14}H_{20}ClGaN_4O_3$
Fw	337.00	361.71	397.51
crystal system	Monoclinic	Orthorhombic	Monoclinic
crystal color	yellow	colorless	colorless
crystal size (mm)	0.12 × 0.18 × 0.18	0.10 × 0.24 × 0.30	0.10 × 0.24 × 0.30
space group	*P*2/*c*	$P2_12_12_1$	$P2_1/n$
a (Å)	20.4818(4)	10.00060(10)	8.4146(2)
b (Å)	10.3924(2)	10.58140(10)	13.5946(3)
c (Å)	12.8076(3)	14.2714(2)	14.3580(3)
α (deg)	90	90	90
β (deg)	101.4985(10)	90	90.7591(8)
γ (deg)	90	90	90
V (Å^3)	2671.45(10)	1510.20(3)	1642.31(6)
Z	8	4	4
D(calcd.) (g/cm^3)	1.631	1.591	1.608
T (K)	150	150	150
wavelength (Å)	0.71073	0.71073	0.71073
F(000)	1368.0	752.0	816.0
reflections collected	5821	3449	16601
unique reflections (R_{int})	3022 (0.026)	3431	3864 (0.037)
R1 ($I > 2s(I)$)	0.0631	0.0209	0.0407
wR2 ($I > 2s(I)$)	0.1348	0.0348	0.0438
R1 (all data)	0.0563	0.0199	0.0277
wR′2 (all data)	0.1317	0.0335	0.0298
Residual electron density (min, max) (e Å^{-3})	−1.47, 1.78	−0.33, 0.26	−0.45, 0.32

Table 2

Selected Bond Lengths (Å) and Angles (deg) in the Determined X-ray Crystal Structures and DFT Optimized Gas Phase Structures of **1**, **2**, **3**, and **4**[a]

	1	2	3	4
	X-ray(esd)/DFT[b]	X-ray(esd)/DFT[c]	X-ray(esd)/DFT[d]	X-ray(esd)/DFT[d]
Metal–N(1)	1.909(4)/1.901	1.825(3)/1.836	2.0367(13)/1.987	1.9538(18)
Metal–N(2)	1.994(4)/2.053	1.923(4)/1.957	2.1210(14)/2.169	2.0589(17)/1.934
Metal–N(3)	1.986(4)/2.053	1.900(4)/1.957	2.1316(13)/2.171	2.0458(18)/2.122
Metal–N(4)	1.901(4)/1.901	1.834(3)/1.836	2.0501(13)/1.983	1.9527(16)/1.935
Zn(1)–O(4)			1.9896(12)/2.2237	
Ga(1)–Cl(X)				2.2060(6)/2.211
C(1)–O(1)	1.255(5)/1.235	1.230(5)/1.234	1.2647(18)/1.238	1.245(3)/1.231
C(7)–O(2)	1.241(6)/1.235	1.247(5)/1.234	1.261(2)/1.239	1.238(3)/1.231
C(1)–N(1)	1.320(6)/1.346	1.342(5)/1.352	1.3125(19)/1.341	1.330(3)/1.349
C(7)–N(4)	1.323(6)/1.346	1.326(5)/1.352	1.317(2)/1.341	1.329(3)/1.348
N(1)–M–N(2)	86.46(16)/86.6	86.75(15)/87.0	81.52(5)/82.6	82.38(7)/81.8
N(2)–M–N(3)	100.09(17)/99.1	99.30(16)/99.3	95.89(5)/96.6	94.88(7)/90.5
N(3)–M–N(4)	86.10(17)/86.6	87.04(14)/87.0	80.76(6)/82.5	83.02(7)/81.8
N(1)–M–N(4)	84.30(16)/85.8	86.37(14)/86.4	79.13(5)/83.9	81.51(7)/83.7
rmsd[e]	0.095	0.154	0.218	0.164

[a] DFT structures were optimized using the B3LYP/6–31 + + G(d,p) methodology with a restricted scheme for nickel, zinc and gallium complexes and an unrestricted scheme for the copper complex.

[b] **1** optimized with C_S symmetry.

[c] The Ni(II) complex was optimized without symmetry constraints but converged with pseudo-C_S symmetry.

[d] The complexes **3** and **4** were optimized without symmetry constraints.

[e] Weighted root-mean square deviation (rmsd) calculated for all heavy atoms between the experimental X-ray crystal structure and the DFT optimized geometries.

Table 3

Calculated One-Electron Reduction and Oxidation Potentials for **1** under Two Solvent Models (H_2O and DMF)

	calcd. $E_{1/2}$/V in water	calcd. $E_{1/2}$/V in DMF	expt./V (SCE) DMF
reduction **1**/[**1**]$^-$	−1.18	−1.46	−1.84
oxidation **1**/[**1**$^{\bullet}$]$^+$ (triplet)	0.14	0.52	0.47